

Doping dependence of the electron-phonon coupling in two families of bilayer superconducting cuprates

Yingying Peng^{1,*}, Leonardo Martinelli^{2,†}, Qizhi Li¹, Matteo Rossi², Matteo Mitrano^{3,‡}, Riccardo Arpaia^{2,4}, Marco Moretti Sala², Qiang Gao⁵, Xuefei Guo³, Gabriella Maria De Luca^{6,7}, Andrew Walters⁸, Abhishek Nag⁸, Andi Barbour⁹, Genda Gu¹⁰, Jonathan Pellicciari⁹, Nicholas B. Brookes¹¹, Peter Abbamonte³, Marco Salluzzo^{6,7}, Xingjiang Zhou⁵, Ke-Jin Zhou⁸, Valentina Bisogni⁹, Lucio Braicovich^{2,11}, Steven Johnston^{12,13,§} and Giacomo Ghiringhelli^{2,14,||}

¹International Center for Quantum Materials, School of Physics, Peking University, Beijing CN-100871, China

²Dipartimento di Fisica, Politecnico di Milano, Piazza Leonardo da Vinci 32, I-20133 Milano, Italy

³Department of Physics and Materials Research Laboratory, University of Illinois, Urbana, Illinois 61801, USA

⁴Quantum Device Physics Laboratory, Department of Microtechnology and Nanoscience, Chalmers University of Technology, SE-41296 Göteborg, Sweden

⁵Beijing National Laboratory for Condensed Matter Physics, Institute of Physics, Chinese Academy of Sciences, Beijing CN-100190, China

⁶Dipartimento di Fisica Ettore Pancini Università di Napoli Federico II, Complesso Monte-Santangelo via Cinthia, I-80126 Napoli, Italy

⁷CNR-SPIN Complesso Monte-Santangelo via Cinthia, I-80126 Napoli, Italy

⁸Diamond Light Source, Harwell Campus, Didcot OX11 0DE, United Kingdom

⁹National Synchrotron Light Source II, Brookhaven National Laboratory, Upton, New York 11973, USA

¹⁰Condensed Matter Physics and Materials Science Department, Brookhaven National Laboratory, Upton, New York 11973, USA

¹¹ESRF—The European Synchrotron, 71 Avenue des Martyrs, CS 40220, F-38043 Grenoble, France

¹²Department of Physics and Astronomy, The University of Tennessee, Knoxville, Tennessee 37996, USA

¹³Institute for Advanced Materials and Manufacturing, University of Tennessee, Knoxville, Tennessee 37996, USA

¹⁴CNR-SPIN, Dipartimento di Fisica, Politecnico di Milano, Piazza Leonardo da Vinci 32, I-20133 Milano, Italy



(Received 9 November 2021; accepted 18 February 2022; published 4 March 2022)

While electron-phonon coupling (EPC) is crucial for Cooper pairing in conventional superconductors, its role in high- T_c superconducting cuprates is debated. Using resonant inelastic x-ray scattering at the oxygen K edge, we study the EPC in $\text{Bi}_2\text{Sr}_2\text{CaCu}_2\text{O}_{8+\delta}$ (Bi2212) and $\text{Nd}_{1+x}\text{Ba}_{2-x}\text{Cu}_3\text{O}_{7-\delta}$ (NBCO) at different doping levels ranging from heavily underdoped ($p = 0.07$) to overdoped ($p = 0.21$). We analyze the data with a localized Lang-Firsov model that allows for the coherent excitations of two phonon modes. While electronic band dispersion effects are non-negligible, we are able to perform a study of the relative values of EPC matrix elements in these cuprate families. In the case of NBCO, the choice of the excitation energy allows us to disentangle modes related to the CuO chains and the CuO_2 planes. Combining the results from the two families, we find the EPC strength decreases with doping at $\mathbf{q}_{\parallel} = (-0.25, 0)$ r.l.u., but has a nonmonotonic trend as a function of doping at smaller momenta. This behavior is attributed to the screening effect of charge carriers. We also find that the phonon intensity is enhanced in the vicinity of the charge-density-wave excitations while the extracted EPC strength appears to be less sensitive to their proximity. By performing a comparative study of two cuprate families, we are able to identify general trends in the EPC for the cuprates and provide experimental input to theories invoking a synergistic role for this interaction in d -wave pairing.

DOI: [10.1103/PhysRevB.105.115105](https://doi.org/10.1103/PhysRevB.105.115105)

I. INTRODUCTION

The pairing interaction in conventional superconductors is mediated by phonons and critically depends on the electron-phonon coupling (EPC) [1,2]. The role played by

EPC in copper-based high critical temperature superconductors (HTSs), however, is still debated. On the one hand, experimental probes like angle-resolved photoemission spectroscopy (ARPES) [3–9] and scanning tunneling microscopy (STM) [10–12] have found evidence for the interplay between lattice vibrations and superconductivity. On the other hand, spin fluctuations are widely believed to provide the dominant contribution to pairing in cuprates [13–15], since the superconducting order parameter is of $d_{x^2-y^2}$ symmetry [16] and superconductivity appears in proximity to antiferromagnetism. This observation, however, does not explicitly rule out a potential role for phonons in pairing. For example, while a complete microscopic picture is currently absent, the interplay

*yingying.peng@pku.edu.cn

†leonardo.martinelli@polimi.it

‡Present address: Department of Physics, Harvard University, Cambridge, Massachusetts 02138, USA.

§sjohn145@utk.edu

||giacomo.ghiringhelli@polimi.it

of the electron-phonon and electron-electron interactions may lead to the enhanced critical temperature (T_c) in HTSs. Indeed, theoretical work has shown that the materials with the largest coupling to the out-of-phase bond-buckling oxygen phonon branch (often referred to as the B_{1g} modes) also have the largest $T_{c,\max}$ [17], suggesting that these modes are relevant to superconductivity.

HTSs have complex phase diagrams that include competing spin-, charge-, and pair-density-waves, a pseudogap, and strange metallic behavior [18–24]. The pivotal parameter that determines the nature of the ground state at a given temperature is the doping p , which gives the number of holes introduced in the CuO_2 planes. In the underdoped region of the phase diagram, the phonon branches are also renormalized in the presence of charge-density-wave (CDW) correlations. This behavior is reminiscent of what happens in conventional metals, where the EPC is the driving force behind the formation of charge modulations [25]. Recent resonant inelastic x-ray scattering (RIXS) studies have indeed observed anomalous softening and enhanced phonon excitations in the vicinity of charge order [26–30].

In the underdoped region of the phase diagram, the coupling between phonon and electrons is also affected by the onset of the pseudogap phase. The pseudogap in HTSs is characterized by a temperature T^* , below which a partial gap opens in the normal state [31]. In general, T^* falls to zero at a critical doping $p_c = 0.19$, where Hall coefficient measurements show a change of carrier density from p to $1 + p$ [32]. Interestingly, a recent ARPES study of $\text{Bi}_2\text{Sr}_2\text{CaCu}_2\text{O}_{8+\delta}$ (Bi2212) revealed a rapid change of bosonic coupling strength to the bond-buckling B_{1g} phonon branch (~ 37 meV) across the pseudogap boundary [8]. To better understand these observations, it is necessary to investigate how EPC changes with doping across the cuprate phase diagram, spanning from the underdoped region to the overdoped Fermi liquid region found for $p > p_c$.

Measuring the full EPC vertex $M(\mathbf{k}, \mathbf{q})$ is challenging, as it can depend on both the fermionic (\mathbf{k}) and bosonic (\mathbf{q}) momenta. Techniques like ARPES probe the \mathbf{k} dependence of the EPC via the electron self-energy, which averages over the phonon momentum \mathbf{q} . Similarly, scattering probes like inelastic x-ray and neutron scattering tend to probe the \mathbf{q} dependence of $M(\mathbf{k}, \mathbf{q})$ via the phonon line width, which averages over the fermion momentum \mathbf{k} . Time-resolved pump-probe optical spectroscopy can extract the electron-boson coupling strength via the relaxation time, but can only access very small \mathbf{q} near the Brillouin zone center [33]. Recently, RIXS has been demonstrated as an effective tool to determine the momentum dependence of the EPC with element specificity, due to the interaction between the excited electrons in the intermediate state and phonons [34]. Since no photoelectron is emitted, RIXS, unlike ARPES, is sensitive to the momentum transfer \mathbf{q} of the phonon and integrates over the fermion momenta \mathbf{k} [35,36]. However, this weighting can be complicated. For example, models have shown that the \mathbf{k} integration can be weighted by other factors like the electron occupations and orbital character of the bands if the system hosts itinerant electrons [34–36]. In cases where the electron mobility can be neglected (e.g., due to a strong core-hole potential), the EPC strength can be extracted from the ratio be-

tween the intensity of the phonon and of its overtones in RIXS spectra [34,37]. Alternatively, one can measure the phonon intensity as the incident beam is detuned from the resonance, as successfully done recently at the $\text{Cu } L_3$ in cuprates [36,38].

Prior RIXS studies of EPC in the 2D cuprates have focused largely on the $\text{Cu } L_3$ edge [30,36,38]. However, it has been established that the bands that cross the Fermi level in doped cuprates have significant oxygen $2p_{x,y}$ orbital character [39]. Moreover, the phonons believed to be most relevant to pairing in the cuprates are the optical oxygen modes [6,17]. It is therefore desirable to also study the EPC at the O K edge in these materials. The RIXS process at this edge involves the $1s \rightarrow 2p$ transition, so in the intermediate state the charge perturbation mostly involves the electron in a $2p$ orbital (plus a core hole, on whose influence we will discuss in the following). Moreover, RIXS experiments at the O K edge can benefit from a better energy resolution and longer-lived core-hole compared to experiments conducted at the $\text{Cu } L_3$ edge [40].

Here, we have studied the coupling between electrons and the oxygen-related phonons in bilayer compounds Bi2212 and $\text{Nd}_{1+x}\text{Ba}_{2-x}\text{Cu}_3\text{O}_{7-\delta}$ (NBCO), using O K -edge RIXS with an energy resolution of about 33 meV. We have extracted the EPC strength from the data using a localized model which is based on a Lang-Firsov transformation (we refer to the model as a Lang-Firsov model in the following) [41–43] that accounts for both bond-buckling and bond-stretching phonons. Combining the results of the two cuprate families, we find that EPC strength decreases with doping at $\mathbf{q}_{\parallel} = (-0.25, 0)$ r.l.u. while this trend becomes nonmonotonic at smaller momenta. The observed changes in the EPC with doping agree with the nonuniform screening effect discussed in theoretical calculations [17]. We have also studied the effect of CDW correlations on EPC. Our results provide experimental insights on the general trends of EPC and allow us to better understand their role in high- T_c cuprate superconductors.

II. METHODS

A. RIXS experiments

We have performed O K -edge RIXS studies on NBCO and Bi2212 samples with different doping levels. The NBCO samples were 100 nm films grown on SrTiO_3 , with two different doping levels: a heavily underdoped sample with $T_c = 38$ K (UD38, $p \simeq 0.07$) and an optimally doped sample with $T_c = 92$ K (OP92, $p \simeq 0.16$). Sample growth description and resistivity measurements of NBCO can be found in the Appendix. Lattice constants were $a = b = 3.9$ Å, while $c = 11.714$ Å in the UD38 sample and $c = 11.74$ Å in the OP one. RIXS spectra were collected at the I21 beamline of the Diamond Light Source [44]. Energy resolution was determined to be 34 meV by measuring the width of the elastic line on a carbon tape. We used a fixed temperature of 20 K.

The Bi2212 samples were single crystals with three doping levels: optimally doped with $T_c = 91$ K (OP91, $p \simeq 0.16$), overdoped with $T_c = 82$ K (OD82, $p \simeq 0.19$), and overdoped with $T_c = 66$ K (OD66, $p \simeq 0.21$). Crystal growth description and magnetization measurements of Bi2212 can be found in the Appendix. The RIXS measurements on Bi2212 were performed using the soft x-ray inelastic beamline (SIX)

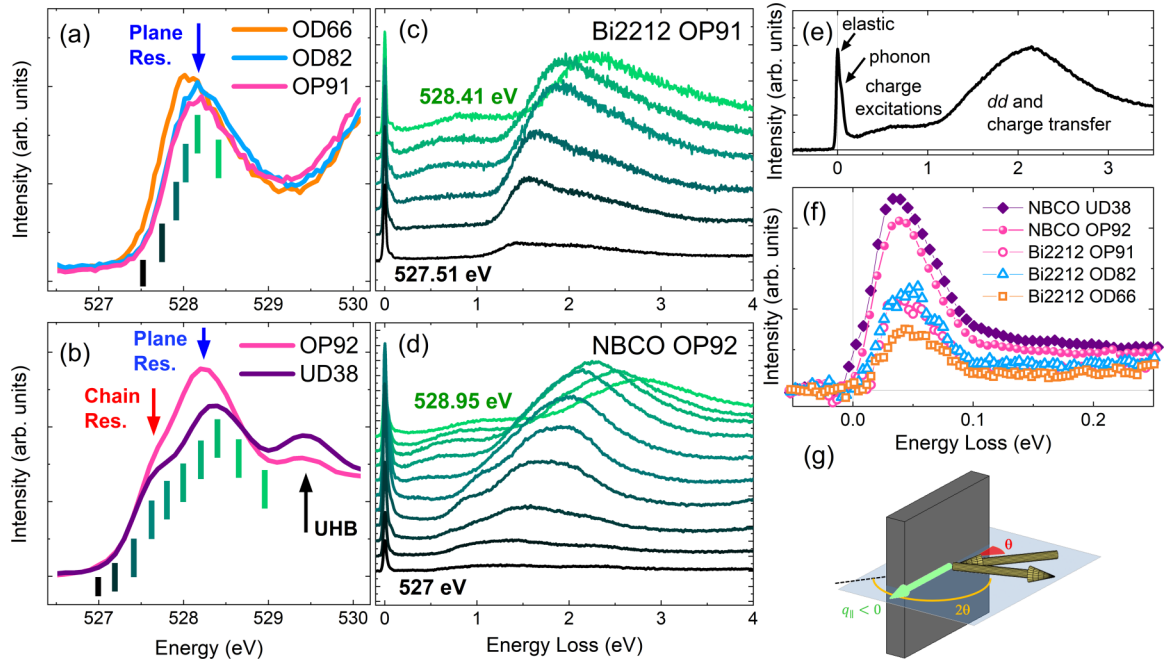


FIG. 1. Overview of data on NBCO and Bi2212 at the O K edge. (a), (b) XAS spectra for different doping values of Bi2212 and NBCO, respectively. The legends indicate the critical temperature of the samples. The relevant resonances are indicated with blue and red arrows. (c), (d) Overview of RIXS spectra in Bi2212 OP91 and NBCO OP92, respectively. The excitation energies for the different spectra are highlighted as ticks in the XAS, using the same color code. (e) Example of RIXS spectrum at oxygen K edge collected on NBCO OP92 at 528.2 eV. Labels indicate the different excitations. (f) Zoom-in of the low-energy regions of RIXS spectra for all the samples acquired at $H = -0.15$ r.l.u. and at the energy corresponding to the plane resonance. The elastic peak has been subtracted for clarity. The spectra have been normalized to the spectral weight between 1 and 7 eV, corresponding to the CT excitation range. (g) Sketch of the experimental geometry. The incoming and outgoing x rays are reported in yellow arrows, and the incident (θ) and scattering (2θ) angles are highlighted. The component of the transferred momentum parallel to the CuO_2 planes is reported in light green.

2-ID at the National Synchrotron Light Source II, Brookhaven National Laboratory [45]. The total experimental energy resolution was ~ 33 meV. We measured at 35 K to minimize sample damage. We define our reciprocal lattice units (r.l.u.) in terms of the tetragonal unit cell with $a = b = 3.8$ Å and $c = 30.89$ Å.

The RIXS spectra were collected with σ incident polarization (perpendicular to the scattering plane) to maximize the charge signal. The scattering angle was fixed at 150° and we used a grazing-in geometry, which by convention means negative parallel transferred momentum \mathbf{q}_{\parallel} , as shown in Fig. 1(g).

B. The Lang-Firsov localized models

The first model developed to describe the EPC in RIXS experiments was the single-site model introduced in Ref. [34] to describe lattice excitations generated at transition metal L edges. The model was derived starting from the local Hamiltonian

$$\mathcal{H} = \epsilon_0 n_d + \omega_0 b^\dagger b + M \sum_{\sigma} n_d (b + b^\dagger), \quad (1)$$

where d_{σ}^{\dagger} and b^{\dagger} represent the creation operators of a spin σ electron and local phonon mode, respectively, $n_d = \sum_{\sigma} d_{\sigma}^{\dagger} d_{\sigma}$, and M is the EPC constant, which is related to a dimensionless coupling parameter $g = (M/\omega_0)^2$. This model is based on the simplifying assumption that both the electrons and phonons are *local* in the sense that they cannot travel through the lattice

at any stage of the RIXS process. In this limit, the RIXS intensity can be computed exactly by use of a Lang-Firsov transformation, yielding

$$I(q, \Omega) = \sum_n |A_n(\Delta + i\Gamma)|^2 \delta(\omega_0 n - \Omega), \quad (2)$$

where Δ is the detuning of the incident energy from the resonant peak, Γ is the half-lifetime of the intermediate state of RIXS process, and

$$A_n(z) = \sum_m \frac{B_{n,m}(g) B_{m,0}(g)}{z - \omega_0(m - g)}, \quad (3)$$

with

$$B_{n,m} = (-1)^n \sqrt{e^{-g} n! m!} \sum_{l=0}^m \frac{(-g)^l g^{\frac{n-m}{2}}}{(m-l)! (n-m+l)!} \quad (4)$$

being the standard Franck-Condon factor ($B_{n,m}$ is understood to mean $B_{\max(n,m), \min(n,m)}$).

Reference [42] recently generalized the single-site model to the case where the localized electron couples to more than one type of phonon. This generalization allows each phonon to be coherently excited and is relevant to the cuprates where we naturally expect coupling to different phonon branches. Here, we consider the case with two types of phonon modes (e.g., the bond-buckling and bond-stretching modes), again

described by the local Hamiltonian [42]

$$\mathcal{H} = \epsilon_0 n_d + \sum_{\lambda=1,2} [\omega_\lambda b_\lambda^\dagger b_\lambda + M_\lambda n_d (b_\lambda + b_\lambda^\dagger)]. \quad (5)$$

The exact RIXS intensity can still be computed, yielding

$$I(q, \Omega) = C_{\text{scale}} \sum_{n_1, n_2} |A_{n_1, n_2}(\Delta + i\Gamma)|^2 \delta\left(\sum_{\lambda=1,2} n_\lambda \omega_\lambda - \Omega\right), \quad (6)$$

where

$$A_{n_1, n_2} = \sum_{m_1, m_2} \frac{D_{n_1, m_1}^{n_2, m_2}(g_1, g_2) D_{m_1, 0}^{m_2, 0}(g_1, g_2)}{\Delta + i\Gamma - \sum_{\lambda=1,2} \omega_\lambda (m_\lambda - g_\lambda)}. \quad (7)$$

Here, C_{scale} is an overall amplitude factor, independent of momentum and detuning and applies to all phonon branches, which we use to scale overall intensity to match the experiment. The coefficients D in Eq. (7) are given by a product of Franck-Condon factors

$$D_{n_1, m_1}^{n_2, m_2}(g_1, g_2) = B_{n_1, m_1}(g_1) B_{n_2, m_2}(g_2), \quad (8)$$

where $g_\lambda = (M_\lambda/\omega_\lambda)^2$.

The model's coupling constants M_λ can be uniquely determined by fitting the energy loss dependence of the lattice excitations and their overtones. Since the relative intensities of the phonon excitations and their overtones are insensitive to an overall scaling of the profile, the prefactor C_{scale} will not affect the extracted coupling constants; however, including this factor allows us to account for additional overall modulations in the intensity (e.g., from overlapping CDW excitations) that are unrelated to the EPC.

We stress that both models neglect all electron mobility involved in the RIXS scattering process. Nevertheless, relatively simple expressions for the RIXS intensity [Eqs. (2) and (6)] are obtained from these approximations that are useful for fitting experimental data. The parameters setting the intensity of phonon excitations in both models are the EPC strength of the different branches g_λ , the detuning energy Δ , and the core-hole lifetime parameter Γ . Throughout, we treat g_λ as a fitting parameter and set Δ based on experimental conditions. We will also fix $\Gamma = 0.15$ eV [36,46,47] for all samples investigated, since the intrinsic lifetime of the state is mostly determined by Auger recombination rate and so independent of the material studied.

A recent theoretical study in the single carrier limit [37] found that the local model for the RIXS cross section produces stronger phonon features in comparison to a fully itinerant model. Moreover, the discrepancy between the models becomes more pronounced as the strength of the localizing core-hole potential is reduced. This result suggests that fitting a localized model to phonon spectra may *underestimate* the strength of the EPC. In the single carrier limit, electron mobility in the intermediate state can also introduce a momentum dependence in the intensity of the phonon excitations that is unrelated to the momentum dependence of the EPC constant $M(\mathbf{k}, \mathbf{q})$. With these caveats in mind, we proceed by fitting the experimental data with the localized model assuming that doing so will allow us to extract general trends in the data. Despite its limitations, this approach has no viable alternatives at present. Other theoretical frameworks either neglect the

strong correlations [35,36], cannot handle multiple phonon branches [47], or cannot treat finite carrier concentrations [37], and it is unclear whether these approximations are more or less drastic than the local approximation when modeling cuprate spectra. Nevertheless, all these theoretical frameworks indicate that the phonon peak intensity is positively correlated with the EPC (with possible additional intensity variations due to effects like orbital character or electron mobility). This result holds independent of the model because phonons are excited by the perturbed charge cloud around the atom during the intermediate state of the RIXS process, and the strength of this interaction is, by definition, the EPC. We therefore proceed while accepting that the absolute values of any extracted couplings should not be uncritically equated to the value entering a microscopic Hamiltonian.

III. EXPERIMENTAL RESULTS

A. RIXS spectra at O *K* edge

The x-ray absorption spectra (XAS) of our Bi2212 and NBCO samples are displayed in Figs. 1(a) and 1(b), respectively. It is easy to identify the Zhang-Rice singlet (ZRS) pre-peak in the O *K*-edge XAS of Bi2212, which originates from the hybridization of the in-plane O $2p_\sigma$ and Cu $3d_{x^2-y^2}$ orbitals [48]. Both the energy and amplitude of the ZRS peak change with doping as expected. On the other hand, we observe two different structures in NBCO whose intensity increases with doping: a main peak at 528.2 eV and another peak at a lower energy (~ 527.6 eV). The former one is associated with doped holes in the CuO₂ planes, while the latter originates from the CuO chains, which act as a charge reservoir in NBCO [48]. Our UD38 sample has short chains in both in-plane directions due to the tetragonal structure, while the OP92 sample has fully developed long chains, and due to the twin structure, they exist in both in-plane directions. The comparison between UD38 and the OP92 sample also nicely highlights the decrease in spectral weight of the upper Hubbard band (UHB) peak around 529.5 eV.

To investigate the electron-phonon interaction, we have acquired RIXS spectra at different incident x-ray energies across the doping-related resonances. Figures 1(c) and 1(d) present an overview of the RIXS spectra for Bi2212 OP91 and NBCO OP92, respectively. The incident energy of each scan is indicated by the tick marks with the same color in Figs. 1(a) and 1(b) for the two compounds. As highlighted in Fig. 1(e), we recognize four features in the spectra: the elastic peak, the phonons (and their overtones) below 0.2 eV, the broad charge excitations peaked around 0.8 eV, and some higher-energy excitations above 1.5 eV from *dd* and charge-transfer (CT) excitations. Moreover, we also identify some spectral weight around 0.5 eV, which could be due to broad bimagnon excitations [49]. To highlight the phonon contribution to the spectra and compare intensities between different samples at resonant energy, we removed the elastic peak and normalized the spectra to their respective *dd*+CT excitations as summarized in Fig. 1(f). The phonon excitations have a larger spectral weight in NBCO and the excitations in Bi2212 OD82 ($p_c = 0.19$) have a stronger intensity than those observed in the OP91 and OD66 samples.

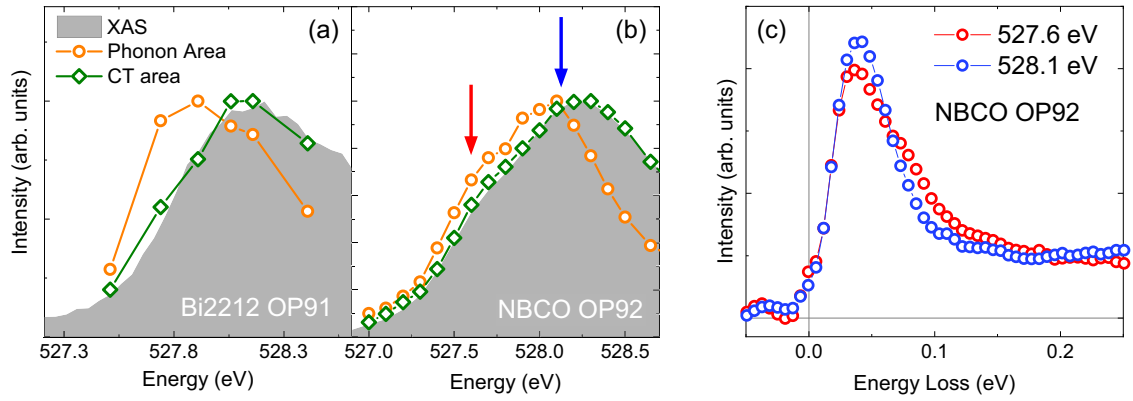


FIG. 2. XAS and phonon resonances in Bi2212 OP91 and NBCO OP92. (a), (b) XAS spectra (grey shade area), the spectral area of phonon (orange circles), and charge-transfer excitations (green diamonds) for Bi2212 OP91 and NBCO OP92, respectively. The red and blue dashed vertical lines indicate the chain and plane resonant energies in NBCO OP92, respectively. (c) RIXS spectra collected at the chain (red) and plane (blue) resonances in NBCO OP92 after subtracting the elastic peaks for comparison.

To precisely determine the resonant energy of the phonon signal (i.e., the energy at which the phonon intensity is maximum), we have extracted their integrated spectral weight. This value was determined by removing the elastic peak and charge excitations from RIXS spectra, and then integrating the infrared region of the RIXS spectra (0–300 meV). As a reference, we have also extracted the spectral weight of CT excitations by integrating the spectra in a 3 eV window centered around their maximum value. The integrated spectral weight of the phonon and CT excitations are plotted in Figs. 2(a) and 2(b) for Bi2212 OP91 and NBCO OP92, respectively, normalized to their maximum value and superimposed over the corresponding XAS spectra. We notice that the one-dimensional breathing mode of the chains has a stronger EPC strength than its two-dimensional counterpart, which is evident from the higher intensity of its first overtone.

The intensity of CT excitations follows closely the XAS spectra in both samples, confirming the stability of our incident energy and the independence of the lifetime of the intermediate state. However, the phonon has a large shift of 200–250 meV relative to the maximum of XAS, both in Bi2212 and NBCO. The presence and magnitude of this energy shift are puzzling. A small displacement, of the order of the phonon energy (≈ 50 – 100 meV) between the maximum of the XAS and the maximum of phonon intensity has been observed before [30,50] and can be accounted for by the localized Lang-Firsov model with a strong EPC and a long core-hole lifetime. The large value observed here, however, requires a different explanation. As suggested in Ref. [51], a possible origin could be a change in the curvature of the potential energy surface between the ground and intermediate state of the RIXS process.

B. Energy detuning measurements

We initially attempted to use the energy detuning method to extract the value of the EPC for the buckling and breathing branches, which has been described in detail in Ref. [36] and has been successfully applied at the Cu L_3 edge [36,38]. This approach is based on the single-site model presented in Sec. II B and consists of acquiring scans at different incident

energies, at and below the resonant peak in the XAS. The EPC of the different phonon branches can then be extracted by fitting the intensities of the different phonon branches (and of their higher harmonics) with Eq. (6). To reduce the number of parameters, we fit all the spectra for a given sample at the same time, using a single overall scale factor and fixing $\Gamma = 0.15$ eV [46,47]. In this way, the only free parameters are the EPC strengths M_λ of the two branches and their energies Ω_λ . We have also subtracted the elastic peaks and considered only the inelastic parts, since the elastic peaks can carry additional contributions from other types of scattering.

As highlighted in Sec. III A, one difficulty is that the maximum of the phonon signal is displaced from the maximum of XAS spectra by ~ 200 – 250 meV. While the employed model can account for a small displacement between the two energies (of the order of ω_λ) in the strong coupling limit, the value of M_λ that is needed is too large and would produce phonon harmonics inconsistent with the RIXS spectra. Therefore, we have decided to artificially put the zero of the detuning in the model at the phonon resonance.

To test the validity of the detuning approach, we have used two different data sets: the chain resonance of NBCO OP92 and the plane resonance of Bi2212 OP91. We chose the chain resonance for NBCO for two reasons. First, it selects the one-dimensional CuO chains as opposed to the two-dimensional CuO₂ planes of Bi2212, which allows us verify whether there are differences related to dimensionality. Second, the chain resonance energy (527.6 eV) is lower than that of the plane (528.2 eV). This difference means that the detuning energies of the chain are not obscured by additional contributions from the plane resonance, while the detuning energies of the plane overlap with the chains.

The spectra with the corresponding fittings are presented in Fig. 3. The solid orange and purple lines are the bond-buckling and bond-stretching phonons including the overtones, respectively, while the green shaded area represents the mixed coherent multiphonons. However, it is evident from the spectra that the detuning method does not reproduce the measured intensities for all incident photon energies. While the agreement is quite good close to the resonance energy for both cases, the calculated spectra far from the resonance signifi-

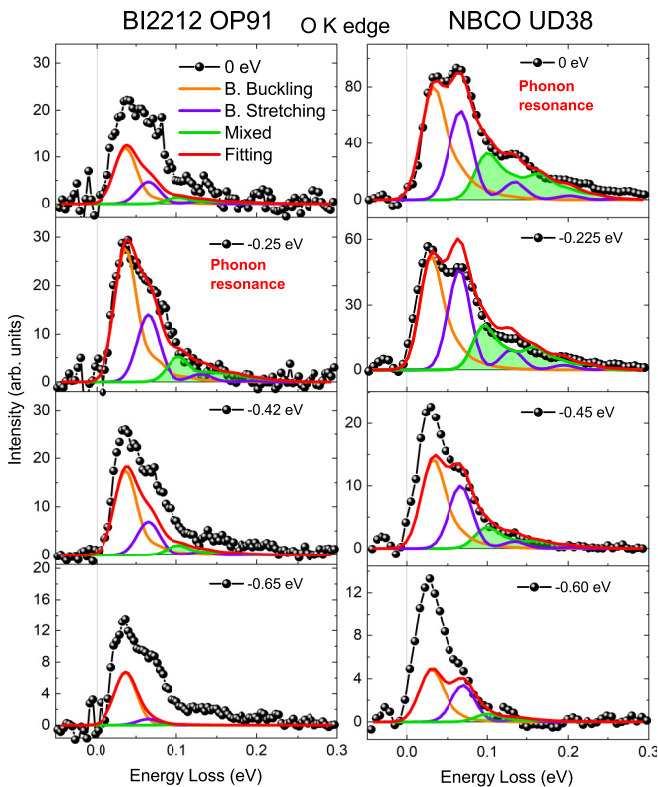


FIG. 3. Detuning data on Bi2212 OP91 (left panels) and NBCO UD38 (right panels). Incident energies were chosen around the plane resonance for Bi2212 OP91 and of chain resonance for NBCO UD38 for the reasons discussed in the text. The momentum transfer was $(-0.15, 0)$ r.l.u. for Bi2212 OP91 and $(-0.25, 0)$ r.l.u. for NBCO UD38. Solid lines are the fitting curves, decomposed into the various phonon branches, obtained through the global fitting discussed in the main text. We have highlighted that, in the case of plane resonance of Bi2212, the phonon resonance is shifted with respect to the maximum of the XAS. A failure of the model is evident at large detuning energies.

cantly underestimate (by more than $\sim 50\%$) the intensity of the phonon branches.

The failure of the detuning method at the ligand K edge is not completely unexpected given the very different nature of the intermediate state between the Cu L_3 and the O K edges, and of the localized assumptions underpinning the Lang-Firsov models. Indeed, at the Cu L_3 edge, the excited electron is more strongly bound to the core hole in comparison to the O K edge. This means that the excited electron is more free to propagate around the lattice during its lifetime in the latter case. Reference [37] recently developed a model for an intermediate state consisting of an itinerant electron interacting with phonons and the core hole in an otherwise empty band. One of the main results derived there is that the detuning curves are quantitatively different from the localized model; they have a weaker dependence on the EPC when the core-hole potentials are weak and they generally decay faster as a function of the detuning energy in comparison to the localized model. We observe a small difference between the decay of the intensity of the two phonon branches with detuning, as evident from Fig. 3. This observation suggests

that the real situation close to the Fermi energy in cuprates is intermediate between the two approaches. Despite the evident failure in reproducing the RIXS spectra at energies away from the resonance, it is still useful, for the subsequent discussion, to report the values of the EPC extracted from this fitting. For optimally doped Bi2212, we obtain $M_1 = 120 \pm 15$ meV and $M_2 = 95 \pm 15$ meV for the buckling and breathing phonon, respectively. Interestingly, these values are actually not far from what has been measured at the Copper L_3 edge [36,38].

C. Effect of doping on EPC

Determining the EPC as a function of doping is crucial for understanding its potential contribution to d -wave pairing. For this purpose, we fit the RIXS spectrum at the resonant energy using Eq. (6), after subtracting the elastic, charge, and CT excitations from the data, as shown in Fig. 4. The size and shape of the elastic peak are determined by measuring the nonresonant spectra of silver paints or carbon tapes following the standard procedure in previous studies [26,29,36,38]. As discussed above, the use of Eq. (6) is likely to underestimate the overall strength of the EPC, particularly at the O K edge, where electron itinerancy in the RIXS intermediate state can be more pronounced than at the Cu L edge [37]. We nevertheless proceed with Eq. (6) in a comparative analysis to identify trends in the data, both as a function of doping and between Bi2212 and NBCO. Presumably, the degree of itinerancy in these systems is comparable for similar doping levels. Thus, the analysis for both samples should be subject to the same systematic error when applying the local model to the data. One should keep in mind that the absolute magnitudes of EPC constants extracted in this analysis cannot be mapped directly onto the $M_\lambda(\mathbf{q})$ entering in any microscopic Hamiltonian.

To fit the data, we consider the coherent contribution from two phonon modes—one from the bond-buckling branch ($\omega_1 \simeq 40$ meV) and one from the bond-stretching branch ($\omega_2 \simeq 70$ meV)—while treating the coupling strengths M_λ as fitting parameters. We also introduce a prefactor C_{scale} , which multiplies the entire spectrum by a constant amount. We are able to obtain a consistent fit to the doping-dependent RIXS spectra using this approach. The doping evolution of the extracted amplitude C_{scale} for the Bi2212 sample are plotted in Figs. 4(c)–4(e) for different momentum transfers, while the corresponding M_λ values are displayed in Figs. 4(f)–4(h). For comparison, we have also overlaid the doping dependence of the phonon amplitude and the extracted M_λ in NBCO at $H = -0.25$ r.l.u. in Figs. 4(c) and 4(f), respectively. Notably, the values of the extracted coupling in Bi2212 and NBCO are almost identical at optimal doping, which provides additional *post hoc* justification for our comparative approach.

For momentum transfer $H = -0.25$ r.l.u., we find that the EPC of the lower-energy buckling mode is stronger than the EPC of the breathing mode in both samples and for all measured doping levels. This observation is consistent with the previous Cu L -edge RIXS measurements on NBCO samples for small momentum transfers [36] and prior ARPES experiments that infer the strongest coupling to the bond-buckling phonon modes [4,6,9,17]. As the hole concentration increases, we find that the extracted M values for both branches decrease monotonically at $H = -0.25$ r.l.u..

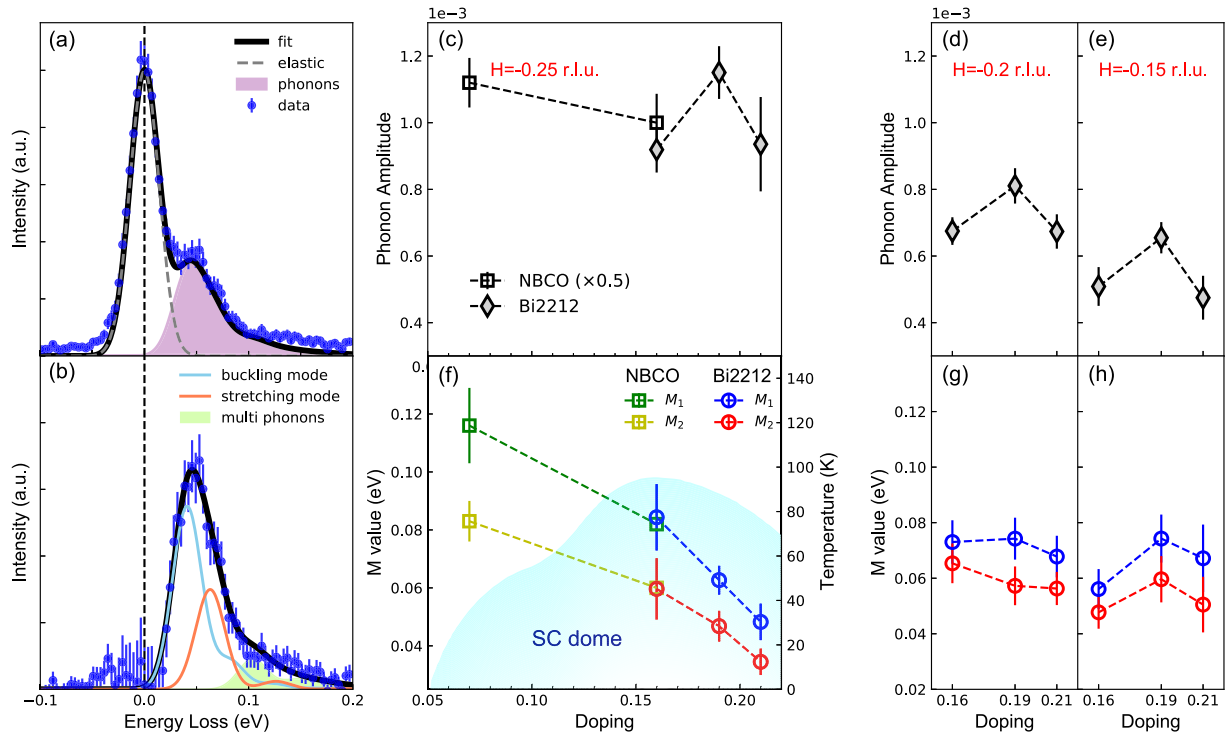


FIG. 4. (a) Fits of RIXS spectra after subtracting the high-energy excitations for Bi2212 OD82, taken at momenta transfer $H = -0.2$ r.l.u.. Elastic peak is fitted by a Gaussian function determined by the energy resolution. The phonon excitations are fitted with the Frank-Condon model considering two phonons, i.e., the buckling mode (~ 40 meV) and stretching mode (~ 70 meV). (b) Phonon components are shown after subtracting the elastic peak. (c)–(e) Doping dependence of phonon amplitude for Bi2212, which shows a maximum at $p_c = 0.19$. The phonon amplitude of NBCO is also shown in (c) and divided a factor of 2 to be close with the data of Bi2212. (f)–(h) Doping dependence of the electron-phonon coupling strengths M for both NBCO and Bi2212. The SC phase diagram [52] of cuprates (shaded area) is displayed in (f).

This behavior can be understood as being a consequence of the improved electronic screening as the system becomes more metallic [17]. The situation is quite different for smaller momenta. For $H = -0.20$ r.l.u., the inferred EPC constants are very weakly dependent on doping, while at $H = -0.15$ r.l.u. the doping dependence even becomes nonmonotonic, with both branches becoming more strongly coupled near $p_c = 0.19$. Interestingly, we notice that the phonon peak amplitude of Bi2212 exhibits a maximum at the pseudogap boundary doping of $p_c = 0.19$, at three momenta. Moreover, an ARPES study of Bi2212 revealed a rapid change of bosonic coupling strength across the pseudogap boundary [8]. Whether the two phenomena are related and what are the underlying reasons for the behavior are still unclear.

The doping dependence summarized here in both compounds is consistent with the poor screening scenario discussed in Ref. [17]. There it was shown that the poor conductivity perpendicular to the CuO_2 plane results in a nonuniform screening of the electron-phonon interaction whereby it was well screened for large momentum transfers but poorly screened at small \mathbf{q} . The suppression of large \mathbf{q} coupling relative to small \mathbf{q} will increase the EPC in the d -wave channel, suggesting that the contribution of these modes to pairing increases as the doping increases and may become largest at optimal doping.

D. Influence of CDW on EPC

Both optimally doped NBCO [53,54] and Bi2212 [55–57] present a CDW ordering with $q_{\text{CDW}} \simeq 0.29$ r.l.u., though the CDW signals become weaker with respect to underdoped samples [54]. Previous RIXS studies at Cu L_3 edge and O K edge on doped cuprates have found an anomalous enhancement of phonon intensity near the CDW wave vector, which is ascribed to the presence of dispersive CDW excitations that overlap and interfere with the phonon excitations [26,29]. We have, therefore, searched for possible enhancements of EPC of buckling and breathing branches due to the presence of charge order.

Employing again the generalized Lang-Firsov model [Eq. (6)] that accounts for coupling to both modes, we have extracted the evolution of the EPC values and the overall scaling prefactor along the $(H, 0)$ direction. Figure 5 shows the momentum dependence of the phonon amplitudes (C_{scale}) and M_λ values in optimally doped Bi2212 and NBCO. Evidently, the phonon amplitudes increase monotonically on approaching the q_{CDW} . At the same time, the EPC does not show a clear trend with M_1 larger than M_2 for all our measured momenta. These results indicate that while the phonon excitations increase in intensity in proximity of q_{CDW} , there is no clear corresponding enhancement in the EPC; this conclusion is also confirmed by the absence of any relative enhance-

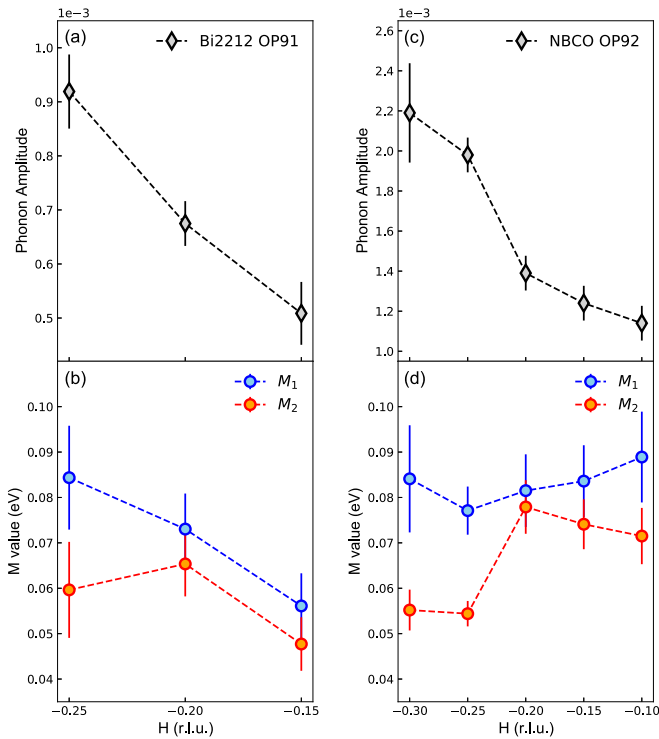


FIG. 5. The momentum dependence of the fitting parameters in Bi2212 OP91 (a), (b) and NBCO OP92 (c), (d). Phonon amplitudes increase with larger \mathbf{q} , while the M values do not show a clear momentum dependence. The extracted M values of two samples are close to one another.

ment of the phonon overtones near the ordering wave vector. One possible explanation is an overlapping contribution to the quasielastic line of CDW fluctuations with finite energy [58]. One should, therefore, be careful in interpreting the bare phonon intensity as the EPC strength in the vicinity of charge instabilities, and the explanation of this discrepancy remains a topic for further investigation.

IV. CONCLUSIONS

We have measured the phonon dynamics in two families of cuprate superconductors as a function of incident energy, momentum, and doping, ranging from strongly underdoped to overdoped samples. Our experimental results highlight that the localized Lang-Firsov model does not describe phonon spectra when the incident energy is detuned away from the resonance peak. We believe that this discrepancy is a fingerprint of an itinerancy of the excited electron and phonon cloud, something which is not captured in the localized model [37]. The detuning method, which has been successfully applied at the Cu L edge to extract the EPC, is therefore not applicable at the O K edge within the present theoretical framework.

By extracting the momentum and doping dependence of EPC measured at resonant x-ray energy, we have revealed a systematic decrease of EPC with increasing doping from strongly underdoped to overdoped samples at high momentum transfer, while closer to the Γ point EPC seems to be less affected by screening, consistent with previous calculations

[17]. We have also detected an anomalous dependence of phonon intensity close to the CDW wave vector. However, we have revealed that momentum dependence of the EPC measured at the O K edge is different from what measured at Cu L edge [36], implying that the RIXS cross section contains additional form factors. The present results show that investigations of the phonon dynamics by O K -edge RIXS in the presence of delocalized electrons has to be made with precautions in the framework of the models developed so far, and new approaches have to be developed to reach a quantitative reliability of results.

ACKNOWLEDGMENTS

Y.Y.P. is grateful for financial support from the Ministry of Science and Technology of China (Grant No. 2019YFA0308401) and the National Natural Science Foundation of China (Grant No. 11974029). P.A. acknowledges support from the Gordon and Betty Moore Foundation, Grant No. GBMF-9452. X.J.Z. thank the financial support from the National Natural Science Foundation of China (Grant No. 11888101), the National Key Research and Development Program of China (Grant no. 2016YFA0300300) and the Strategic Priority Research Program (B) of the Chinese Academy of Sciences (Grant no. XDB25000000). S.J. is supported by the National Science Foundation under Grant No. DMR-1842056. L.M., M.M.S. and G.G. acknowledge support by the project PRIN2017 "Quantum-2D" ID 2017Z8TS5B of the Ministry for University and Research (MIUR) of Italy. R.A. acknowledges support by the Swedish Research Council (VR) under the Project 2020-04945. This research used Diamond Light Source beam line I21 under the proposal SP20012. N.B.B. thanks Diamond Light Source for hosting him at the time the experiment was carried out at I21. This research used the beamline 2-ID of the National Synchrotron Light Source II, a U.S. Department of Energy (DOE) Office of Science User Facility operated for the DOE Office of Science by Brookhaven National Laboratory under Contract No. DE-SC0012704. The work at BNL was supported by the US Department of Energy, office of Basic Energy Sciences, Contract No. DOE-sc0012704.

APPENDIX

Sample characterization

NBCO samples were prepared as described in Refs. [59,60]. Epitaxial thin films were deposited by high oxygen pressure diode sputtering on $10 \times 10 \text{ mm}^2$ SrTiO₃(100) single crystals. The substrates were etched in a BHF solution (pH = 5.5) and annealed at 950 °C in 10 Torr of pure oxygen.

Optimally and underdoped NBCO films were deposited using targets of Nd_{0.97}Ba_{2.03}Cu₃O₇ and Nd_{1.2}Ba_{1.8}Cu₃O₇, respectively. The Nd excess at the Ba site gives rise to a reduced hole-carrier concentration and to underdoping, but structural and morphological properties of the films are similar to the optimally doped films. The films were deposited in an atmosphere composed of 95% of oxygen and 5% argon, at a pressure of 1.7 Torr. The deposition temperature was 920 °C and the growth rate was about 0.01 nm s⁻¹. Subsequently, the temperature was reduced to 500 °C while keeping the pressure

constant and the chamber was filled with 400 Torr of pure oxygen. The samples were then annealed in this condition to reach full oxygenation. The rocking curves around the (001) and (005) reflections of all films deposited are characterized by a FWHM of 0.03° and 0.08° , respectively, comparable with the resolution of our diffractometer [59]. This result indicates a very small orientation misalignment between individual islands in each sample. The structural coherence along the c axis of the NBCO films extends to the entire thickness, as demonstrated by the presence of well-defined Pendellösung fringes around the (001) peak, even for films thicker than 100 nm. More details can be found in Refs. [59–61]. The resistance of the NBCO samples is reported in Fig. 6(a) as a function of temperature, highlighting the superconducting transition temperature T_c .

Optimally doped $\text{Bi}_2\text{Sr}_2\text{CaCu}_2\text{O}_{8+\delta}$ (Bi2212, OP91) single crystals were grown by the traveling solvent floating zone method [62,63]. Overdoped Bi2212 samples were prepared by annealing the optimally doped sample in a high-pressure oxygen atmosphere [64]. The overdoped Bi2212 sample with $T_c \sim 82$ K (OD82) was obtained by annealing in 0.2 Mpa oxygen at 500°C for five days. The heavily overdoped Bi2212 sample with $T_c \sim 66$ K (OD66) was obtained by annealing in 12 Mpa oxygen at 550°C for five days. All samples have high quality which exhibit sharp superconducting transitions with a transition width of ~ 2 K, as shown in Fig. 6(b). The temperature dependence of the AC magnetic susceptibility was measured using a Quantum Design MPMS XL-1 system with a low magnetic field of 1 Oe.

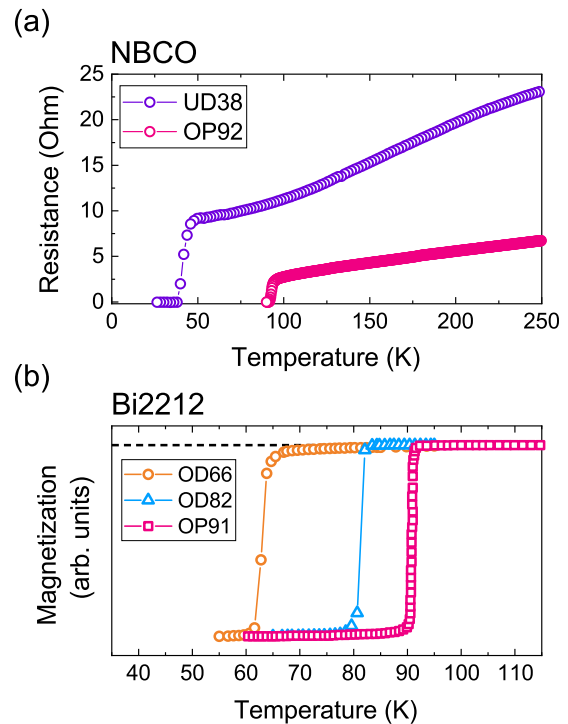


FIG. 6. (a) Resistance of the underdoped and optimally doped NBCO epitaxial films as a function of temperature. (b) Magnetization measurements of the Bi2212 single crystals as a function of temperature in a magnetic field of 1 Oe. The horizontal dashed line is the zero of magnetization.

- [1] J. Bardeen, L. N. Cooper, and J. R. Schrieffer, *Phys. Rev.* **108**, 1175 (1957).
- [2] W. L. McMillan and J. M. Rowell, *Phys. Rev. Lett.* **14**, 108 (1965).
- [3] A. Lanzara, P. V. Bogdanov, X. J. Zhou, S. A. Kellar, D. L. Feng, E. D. Lu, T. Yoshida, H. Eisaki, A. Fujimori, K. Kishio, J.-I. Shimoyama, T. Noda, S. Uchida, Z. Hussain, and Z.-X. Shen, *Nature (London)* **412**, 510 (2001).
- [4] T. Cuk, F. Baumberger, D. H. Lu, N. Ingle, X. J. Zhou, H. Eisaki, N. Kaneko, Z. Hussain, T. P. Devereaux, N. Nagaosa, and Z.-X. Shen, *Phys. Rev. Lett.* **93**, 117003 (2004).
- [5] T. P. Devereaux, T. Cuk, Z.-X. Shen, and N. Nagaosa, *Phys. Rev. Lett.* **93**, 117004 (2004).
- [6] T. Cuk, D. H. Lu, X. J. Zhou, Z.-X. Shen, T. P. Devereaux, and N. Nagaosa, *Phys. Status Solidi B* **242**, 11 (2005).
- [7] J. Graf, M. d’Astuto, C. Jozwiak, D. R. Garcia, N. L. Saini, M. Krisch, K. Ikeuchi, A. Q. R. Baron, H. Eisaki, and A. Lanzara, *Phys. Rev. Lett.* **100**, 227002 (2008).
- [8] Y. He, M. Hashimoto, D. Song, S.-D. Chen, J. He, I. M. Vishik, B. Moritz, D.-H. Lee, N. Nagaosa, J. Zaanen, T. P. Devereaux, Y. Yoshida, H. Eisaki, D. H. Lu, and Z.-X. Shen, *Science* **362**, 62 (2018).
- [9] S. Johnston, I. M. Vishik, W. S. Lee, F. Schmitt, S. Uchida, K. Fujita, S. Ishida, N. Nagaosa, Z. X. Shen, and T. P. Devereaux, *Phys. Rev. Lett.* **108**, 166404 (2012).
- [10] J. Lee, K. Fujita, K. McElroy, J. A. Slezak, M. Wang, Y. Aiura, H. Bando, M. Ishikado, T. Masui, J. X. Zhu, A. V. Balatsky, H. Eisaki, S. Uchida, and J. C. Davis, *Nature (London)* **442**, 546 (2006).
- [11] G. Zhao, *Phys. Rev. Lett.* **103**, 236403 (2009).
- [12] G. Zhao, *Phys. Rev. B* **75**, 214507 (2007).
- [13] N. Bulut and D. J. Scalapino, *Phys. Rev. B* **54**, 14971 (1996).
- [14] T. A. Maier, D. Poilblanc, and D. J. Scalapino, *Phys. Rev. Lett.* **100**, 237001 (2008).
- [15] D. J. Scalapino, *Rev. Mod. Phys.* **84**, 1383 (2012).
- [16] C. C. Tsuei and J. R. Kirtley, *Rev. Mod. Phys.* **72**, 969 (2000).
- [17] S. Johnston, F. Vernay, B. Moritz, Z.-X. Shen, N. Nagaosa, J. Zaanen, and T. P. Devereaux, *Phys. Rev. B* **82**, 064513 (2010).
- [18] E. Fradkin, S. A. Kivelson, and J. M. Tranquada, *Rev. Mod. Phys.* **87**, 457 (2015).
- [19] B. Keimer, S. A. Kivelson, M. R. Norman, S. Uchida, and J. Zaanen, *Nature (London)* **518**, 179 (2015).
- [20] R. Comin and A. Damascelli, *Annu. Rev. Condens. Matter Phys.* **7**, 369 (2016).
- [21] D. F. Agterberg, J. S. Davis, S. D. Edkins, E. Fradkin, D. J. Van Harlingen, S. A. Kivelson, P. A. Lee, L. Radzihovsky, J. M. Tranquada, and Y. Wang, *Annu. Rev. Condens. Matter Phys.* **11**, 231 (2020).
- [22] R. Arpaia, E. Andersson, E. Tralbaldo, T. Bauch, and F. Lombardi, *Phys. Rev. Mater.* **2**, 024804 (2018).

- [23] R. Arpaia and G. Ghiringhelli, *J. Phys. Soc. Jpn.* **90**, 111005 (2021).
- [24] E. Wahlberg, R. Arpaia, G. Seibold, M. Rossi, R. Fumagalli, E. Trabaldo, N. B. Brookes, L. Braicovich, S. Caprara, U. Gran, G. Ghiringhelli, T. Bauch, and F. Lombardi, *Science* **373**, 1506 (2021).
- [25] X. Zhu, Y. Cao, J. Zhang, E. W. Plummer, and J. Guo, *Proc. Natl. Acad. Sci. USA* **112**, 2367 (2015).
- [26] L. Chaix, G. Ghiringhelli, Y. Y. Peng, M. Hashimoto, B. Moritz, K. Kummer, N. B. Brookes, Y. He, S. Chen, S. Ishida, Y. Yoshida, H. Eisaki, M. Salluzzo, L. Braicovich, Z.-X. Shen, T. P. Devereaux, and W.-S. Lee, *Nat. Phys.* **13**, 952 (2017).
- [27] H. Miao, D. Ishikawa, R. Heid, M. Le Tacon, G. Fabbris, D. Meyers, G. D. Gu, A. Q. R. Baron, and M. P. M. Dean, *Phys. Rev. X* **8**, 011008 (2018).
- [28] J. Q. Lin, H. Miao, D. G. Mazzone, G. D. Gu, A. Nag, A. C. Walters, M. García-Fernández, A. Barbour, J. Pellicciari, I. Jarrige, M. Oda, K. Kurosawa, N. Momono, K.-J. Zhou, V. Bisogni, X. Liu, and M. P. M. Dean, *Phys. Rev. Lett.* **124**, 207005 (2020).
- [29] J. Li, A. Nag, J. Pellicciari, H. Robarts, A. Walters, M. Garcia-Fernandez, H. Eisaki, D. Song, H. Ding, S. Johnston, R. Comin, and K.-J. Zhou, *Proc. Natl. Acad. Sci. USA* **117**, 16219 (2020).
- [30] Y. Y. Peng, A. A. Husain, M. Mitrano, S. X.-L. Sun, T. A. Johnson, A. V. Zakrzewski, G. J. MacDougall, A. Barbour, I. Jarrige, V. Bisogni, and P. Abbamonte, *Phys. Rev. Lett.* **125**, 097002 (2020).
- [31] T. Timusk and B. Statt, *Rep. Prog. Phys.* **62**, 61 (1999).
- [32] S. Badoux, W. Tabis, F. Laliberté, G. Grissonnache, B. Vignolle, D. Vignolles, J. Béard, D. Bonn, W. Hardy, R. Liang *et al.*, *Nature (London)* **531**, 210 (2016).
- [33] E. E. M. Chia, D. Springer, S. K. Nair, X. Zou, S. A. Cheong, C. Panagopoulos, T. Tamegai, H. Eisaki, S. Ishida, S. ichi Uchida, A. J. Taylor, and J.-X. Zhu, *New J. Phys.* **15**, 103027 (2013).
- [34] L. J. P. Ament, M. van Veenendaal, and J. van den Brink, *Europhys. Lett.* **95**, 27008 (2011).
- [35] T. P. Devereaux, A. M. Shvaika, K. Wu, K. Wohlfeld, C. J. Jia, Y. Wang, B. Moritz, L. Chaix, W.-S. Lee, Z.-X. Shen, G. Ghiringhelli, and L. Braicovich, *Phys. Rev. X* **6**, 041019 (2016).
- [36] L. Braicovich, M. Rossi, R. Fumagalli, Y. Peng, Y. Wang, R. Arpaia, D. Betto, G. M. De Luca, D. Di Castro, K. Kummer, M. Moretti Sala, M. Pagetti, G. Balestrino, N. B. Brookes, M. Salluzzo, S. Johnston, J. van den Brink, and G. Ghiringhelli, *Phys. Rev. Res.* **2**, 023231 (2020).
- [37] K. Bieniasz, S. Johnston, and M. Berciu, *SciPost Phys.* **11**, 62 (2021).
- [38] M. Rossi, R. Arpaia, R. Fumagalli, M. Moretti Sala, D. Betto, K. Kummer, G. M. De Luca, J. van den Brink, M. Salluzzo, N. B. Brookes, L. Braicovich, and G. Ghiringhelli, *Phys. Rev. Lett.* **123**, 027001 (2019).
- [39] C. T. Chen, F. Sette, Y. Ma, M. S. Hybertsen, E. B. Stechel, W. M. C. Foulkes, M. Schluter, S.-W. Cheong, A. S. Cooper, L. W. Rupp, B. Batlogg, Y. L. Soo, Z. H. Ming, A. Krol, and Y. H. Kao, *Phys. Rev. Lett.* **66**, 104 (1991).
- [40] N. B. Brookes, F. Yakhov-Harris, K. Kummer, A. Fondacaro, J. Cezar, D. Betto, E. Velez-Fort, A. Amorese, G. Ghiringhelli, L. Braicovich, R. Barrett, G. Berruyer, F. Cianciosi, L. Eybert, P. Marion, P. van der Linden, and L. Zhang, *Nucl. Instr. Meth. Phys. Res. A* **903**, 175 (2018).
- [41] I. G. Lang and Y. A. Firsov, *Sov. Phys. JETP* **16**, 1301 (1963).
- [42] A. Geondzhian and K. Gilmore, *Phys. Rev. B* **101**, 214307 (2020).
- [43] A. Geondzhian, A. Sambri, G. M. De Luca, R. Di Capua, E. Di Gennaro, D. Betto, M. Rossi, Y. Y. Peng, R. Fumagalli, N. B. Brookes, L. Braicovich, K. Gilmore, G. Ghiringhelli, and M. Salluzzo, *Phys. Rev. Lett.* **125**, 126401 (2020).
- [44] K.-J. Zhou, A. Walters, M. Garcia-Fernandez, T. Rice, M. Hand, A. Nag, J. Li, S. Agrestini, P. Garland, H. Wang, S. Alcock, I. Nistea, B. Nutter, N. Rubies, G. Knap, M. Gaughran, F. Yuan, P. Chang, J. Emmins, and G. Howell, *J. Synchrotron Rad.* **29**, 563 (2022).
- [45] I. Jarrige, V. Bisogni, Y. Zhu, W. Leonhardt, and J. Dvorak, *Synchrotron Radiat. News* **31**, 7 (2018).
- [46] W. S. Lee, S. Johnston, B. Moritz, J. Lee, M. Yi, K. J. Zhou, T. Schmitt, L. Patthey, V. Strocov, K. Kudo, Y. Koike, J. van den Brink, T. P. Devereaux, and Z. X. Shen, *Phys. Rev. Lett.* **110**, 265502 (2013).
- [47] S. Johnston, C. Monney, V. Bisogni, K.-J. Zhou, R. Kraus, G. Behr, V. N. Strocov, J. Málek, S.-L. Drechsler, J. Geck, T. Schmitt, and J. van den Brink, *Nat. Commun.* **7**, 10563 (2016).
- [48] D. G. Hawthorn, K. M. Shen, J. Geck, D. C. Peets, H. Wadati, J. Okamoto, S.-W. Huang, D. J. Huang, H.-J. Lin, J. D. Denlinger, R. Liang, D. A. Bonn, W. N. Hardy, and G. A. Sawatzky, *Phys. Rev. B* **84**, 075125 (2011).
- [49] V. Bisogni, L. Simonelli, L. J. P. Ament, F. Forte, M. Moretti Sala, M. Minola, S. Huotari, J. van den Brink, G. Ghiringhelli, N. B. Brookes, and L. Braicovich, *Phys. Rev. B* **85**, 214527 (2012).
- [50] X. Feng, S. Sallis, Y.-C. Shao, R. Qiao, Y.-S. Liu, L. C. Kao, A. S. Tremsin, Z. Hussain, W. Yang, J. Guo, and Y.-D. Chuang, *Phys. Rev. Lett.* **125**, 116401 (2020).
- [51] A. Geondzhian and K. Gilmore, *Phys. Rev. B* **98**, 214305 (2018).
- [52] L. Taillefer, *Annu. Rev. Condens. Matter Phys.* **1**, 51 (2010).
- [53] G. Ghiringhelli, M. Le Tacon, M. Minola, S. Blanco-Canosa, C. Mazzoli, N. B. Brookes, G. M. De Luca, A. Frano, D. G. Hawthorn, F. He, T. Loew, M. M. Sala, D. C. Peets, M. Salluzzo, E. Schierle, R. Sutarto, G. A. Sawatzky, E. Weschke, B. Keimer, and L. Braicovich, *Science* **337**, 821 (2012).
- [54] S. Blanco-Canosa, A. Frano, E. Schierle, J. Porras, T. Loew, M. Minola, M. Bluschke, E. Weschke, B. Keimer, and M. Le Tacon, *Phys. Rev. B* **90**, 054513 (2014).
- [55] M. Hashimoto, G. Ghiringhelli, W.-S. Lee, G. Dellea, A. Amorese, C. Mazzoli, K. Kummer, N. B. Brookes, B. Moritz, Y. Yoshida, H. Eisaki, Z. Hussain, T. P. Devereaux, Z.-X. Shen, and L. Braicovich, *Phys. Rev. B* **89**, 220511(R) (2014).
- [56] E. H. da Silva Neto, P. Aynajian, A. Frano, R. Comin, E. Schierle, E. Weschke, A. Gyenis, J. Wen, J. Schneeloch, Z. Xu, S. Ono, G. Gu, M. Le Tacon, and A. Yazdani, *Science* **343**, 393 (2014).
- [57] W. S. Lee, K.-J. Zhou, M. Hepting, J. Li, A. Nag, A. C. Walters, M. Garcia-Fernandez, H. C. Robarts, M. Hashimoto, H. Lu, B. Noszarzewski, D. Song, H. Eisaki, Z. X. Shen, B. Moritz, J. Zaanen, and T. P. Devereaux, *Nat. Phys.* **17**, 53 (2021).
- [58] R. Arpaia, S. Caprara, R. Fumagalli, G. De Vecchi, Y. Y. Peng, E. Andersson, D. Betto, G. M. De Luca, N. B. Brookes, F. Lombardi, M. Salluzzo, L. Braicovich, C. Di Castro, M. Grilli, and G. Ghiringhelli, *Science* **365**, 906 (2019).

- [59] M. Salluzzo, G. De Luca, R. Di Capua, A. Gambardella, Z. Ristic, and R. Vaglio, *Supercond. Sci. Technol.* **22**, 034010 (2009).
- [60] G. De Luca, G. Ausanio, M. Salluzzo, and R. Vaglio, *Supercond. Sci. Technol.* **18**, 791 (2005).
- [61] M. Salluzzo, G. M. de Luca, D. Marrè, M. Putti, M. Tropeano, U. Scotti di Uccio, and R. Vaglio, *Phys. Rev. B* **72**, 134521 (2005).
- [62] B. Liang and C. T. Lin, *J. Cryst. Growth* **237**, 756 (2002).
- [63] J. S. Wen, Z. J. Xu, G. Y. Xu, M. Hücker, J. M. Tranquada, and G. D. Gu, *J. Cryst. Growth* **310**, 1401 (2008).
- [64] Y.-X. Zhang, L. Zhao, G.-D. Gu, and X.-J. Zhou, *Chin. Phys. Lett.* **33**, 067403 (2016).